Mutations in Potassium Channel KCND3 Cause Spinocerebellar Ataxia Type 19

Duarri, Anna; Jezierska, Justyna; Fokkens, Michiel; Meijer, Michel; Schelhaas, Helenius J; den Dunnen, Wilfred F A; van Dijk, Freerk; Verschuuren - Bemelmans, Cornelia; Hageman, Gerard; van de Vlies, Pieter

Published in:
Annals of Neurology

DOI:
10.1002/ana.23700

Publication date:
2012

Mutations in Potassium Channel *KCND3* Cause Spinocerebellar Ataxia Type 19

Anna Duarri, PhD,[1] Justyna Jezierska, MSc,[1] Michiel Fokkens, BSc,[1] Michel Meijer, BSc,[2] Helenius J. Schelhaas, MD, PhD,[3] Wilfred F. A. den Dunnen, MD, PhD,[4] Freerk van Dijk, BSc,[5] Corien Verschuuren-Bemelmans, MD,[1] Gerard Hageman, MD,[6] Pieter van de Vlies, BSc,[1] Benno Küsters, MD, PhD,[7] Bart P. van de Warrenburg, MD, PhD,[3] Berry Kremer, MD, PhD,[8] Cisca Wijmenga, PhD,[1] Richard J. Sinke, PhD,[1] Morris A. Swertz, PhD,[4] Harm H. Kampinga, PhD,[9] Erik Boddeke, PhD,[2] and Dineke S. Verbeek, PhD[1]

Objective: To identify the causative gene for the neurodegenerative disorder spinocerebellar ataxia type 19 (SCA19) located on chromosomal region 1p21-q21.
Methods: Exome sequencing was used to identify the causal mutation in a large SCA19 family. We then screened 230 ataxia families for mutations located in the same gene (*KCND3*, also known as Kv4.3) using high-resolution melting. SCA19 brain autopsy material was evaluated, and in vitro experiments using ectopic expression of wild-type and mutant Kv4.3 were used to study protein localization, stability, and channel activity by patch-clamping.
Results: We detected a T352P mutation in the third extracellular loop of the voltage-gated potassium channel *KCND3* that cosegregated with the disease phenotype in our original family. We identified 2 more novel missense mutations in the channel pore (M373I) and the S6 transmembrane domain (S390N) in 2 other ataxia families. T352P cerebellar autopsy material showed severe Purkinje cell degeneration, with abnormal intracellular accumulation and reduced protein levels of Kv4.3 in their soma. Ectopic expression of all mutant proteins in HeLa cells revealed retention in the endoplasmic reticulum and enhanced protein instability, in contrast to wild-type Kv4.3 that was localized on the plasma membrane. The regulatory β subunit Kv channel interacting protein 2 was able to rescue the membrane localization and the stability of 2 of the 3 mutant Kv4.3 complexes. However, this either did not restore the channel function of the membrane-located mutant Kv4.3 complexes or restored it only partially.
Interpretation: *KCND3* mutations cause SCA19 by impaired protein maturation and/or reduced channel function.

ANN NEUROL 2012;72:870–880

Patients with a dominantly inherited spinocerebellar ataxia (SCA) are characterized by a late onset, progressive atrophy of the cerebellum, affecting their motor coordination, balance, speech, and eye coordination movements, with many other symptoms.[1] To date, 36 SCA loci have been described; for 21 of these, the corresponding disease gene and causative mutation have been identified.[1–4] The majority of SCAs represent repeat expansion diseases, including a coding CAG repeat (SCA1–3, 6, 7, and 17) causing misfolding of the encoding protein due to the expanded polyglutamine tracts, or groups of noncoding CAG, CTG, ATTCT, and GGCCTG repeats (SCA8, 10, 12, and 36), or large TGGAA repeat insertions (SCA31) that induce RNA-

View this article online at wileyonlinelibrary.com. DOI: 10.1002/ana.23700

Received Apr 5, 2012, and in revised form May 21, 2012. Accepted for publication Jun 13, 2012.

Address correspondence to Prof Verbeek, Correspondence to: Department of Genetics, University Medical Center Groningen, P.O. Box 30001, 9700 RB Groningen, the Netherlands. E-mail: D.S.Verbeek@umcg.nl

From the [1]Department of Genetics, University of Groningen, University Medical Center Groningen, Groningen; [2]Department of Medical Physiology, University Medical Center Groningen, Groningen; [3]Department of Neurology, Donders Institute for Brain, Cognition, and Behavior, Center for Neuroscience, Radboud University Nijmegen Medical Center, Nijmegen; [4]Department Pathology and Medical Biology, University of Groningen, University Medical Center Groningen, Groningen; [5]Genomics Coordination Center, Department of Genetics, University Medical Center Groningen and Groningen Bioinformatics Center, University of Groningen, Groningen; [6]Department of Neurology, Medical Spectrum Twente, Enschede; [7]Department of Pathology, Radboud University Nijmegen Medical Center, Nijmegen; [8]Department of Neurology, University Medical Center Groningen, Groningen; [9]Department of Cell Biology, Section of Radiation and Stress Cell Biology, University Medical Center Groningen, University of Groningen, Groningen, the Netherlands.

Additional supporting information can be found in the online version of this article.

mediated gain-of-function mechanisms.[1] The remaining known SCA types are caused by missense mutations or chromosomal rearrangements (SCA5, 11, 13–15, 20, 23, 27, 28, 31, and 35) in genes displaying a wide range of protein functions, often causing alterations in synaptic transmission via calcium, potassium, and glutamate signaling.[1,5–7]

We previously mapped SCA19 in a large Dutch family (4 generations with 13 affected members) to a region of approximately 38 Mb located in chromosomal region 1p21-q21.[8] The SCA19 locus shows significant overlap with the SCA22 locus later reported in a single Chinese family,[9] suggesting that SCA19 and SCA22 might be caused by mutations in the same gene and lead to an ataxia type with a worldwide distribution.[10] Clinical investigation and magnetic resonance imaging of our SCA19 family revealed a relatively mild, cerebellar ataxic syndrome with cognitive impairment, pyramidal tract involvement, tremor and peripheral neuropathy, and mild atrophy of the cerebellar hemispheres and vermis.[11] The SCA19 locus comprises some 500 genes and transcripts, but we could not identify the causative gene and mutation by candidate gene sequencing (data unpublished). We therefore applied exome sequencing to 2 affected family members and identified a novel missense mutation in *KCND3* (also known as Kv4.3) as causing SCA19 in our family.[8] Later we identified 2 different missense mutations in this gene in 2 other families from our Dutch ataxia cohort. Kv4.3 is a Shal-related subfamily, voltage-gated potassium channel, involved in the transient outward A-type K^+ current in the neurons. It is highly expressed in the cerebellum.[12–14] The 3 mutations in *KCND3* either impaired proper endoplasmic reticulum (ER)–Golgi membrane trafficking and/or reduced Kv4.3 channel functioning. Together, our genetic and functional studies provide evidence that mutations in *KCND3* cause SCA19.

Subjects and Methods

Subjects

The participants of our original SCA19 family all gave informed written consent, as required by the Medical Ethics Committee of the University Medical Center Utrecht, the Netherlands. The additional 230 ataxia patients screened in this study were obtained from the Genome analysis laboratory, Department of Genetics, University Medical Center Groningen. All extended DNA analyses were performed in a diagnostic setting (accredited diagnostic DNA lab). Only DNA samples from patients who were referred for genetic testing for SCA1–3, 6–12, 14, and 17 were used. The additional tests were thus performed in line with the original diagnostic request. Moreover, patients were asked whether they agreed to their DNA being used for future (anonymous) studies to help develop or improve diagnostics. If they objected, this was indicated on the original Request for DNA Test form, and their DNA was not used. The unrelated 400 control individuals were obtained from the Dutch blood bank. DNA was extracted from peripheral blood by a routine salting-out procedure.

Exome Sequencing and Mutation Screening

The genomic DNA samples (individuals IV:1 and II:10 marked by an *asterisk* in pedigree 1, Supplementary Fig 1A) were randomly fragmented using nebulization. The resulting fragments were bar-coded, using the standard NEBNext DNA Library Prep Master Mix Set for Illumina (New England Biolabs, Ipswich, MA). Fragments with an average insert size of 220bp were amplified by polymerase chain reaction (PCR), and the quality was verified on an Experion machine (Bio-Rad, Richmond, CA). Exome capturing was performed using the Agilent SureSelect All exon V2 kit. After PCR amplification of the enriched products, paired-end sequencing was performed on a HiSeq2000 (Illumina, San Diego, CA) with 100bp reads. Image files were processed using standard Illumina base-calling software, and the generated reads were ready for downstream processing after demultiplexing.

The reads were aligned to the human reference genome, build 37, using BWA software.[15] To clean the aligned data and perform variant calling, we applied Picard duplicate removal and the Genome Analysis Toolkit,[16,17] containing quality score recalibration, indel realignment, and an unified genotyper. Using snpEff (http://snpeff.sourceforge.net), the variants were annotated with information from dbSNP132, 1000 Genomes Project (phases 1, 2, and 3), and Ensembl, build 37.64. These programs are all integrated in our MOLGENIS Compute analysis pipeline developed by the Genomics Coordination Center, Department of Genetics, University of Groningen (http://wiki.gcc.rug.nl/wiki/GccStart).[18] Pathogenicity predictions for variants were obtained from PolyPhen 2.0, SIFT, and Align GVD.[19–23] Variations were validated by direct Sanger sequencing and analyzed using DNA Variant Analysis Software Mutation Surveyor. The high-resolution melting technology with the LightScanner (Idaho Technologies, Salt Lake City, UT) was used to identify additional mutations in *KCND3* according to the manufacturer's instructions. The primers used to amplify the amplicons are listed in Supplementary Table 1. Aberrant melting curves were checked by direct Sanger sequencing, and the sequences were aligned to reference sequence NM_172198.

Postmortem Human Brain Specimens

SCA19 cerebellar tissue (hemispheres and vermis) from the patient (individual II:1 in pedigree 1 in Supplementary Fig 1A) with a T352P mutation and an age-matched, nondegenerative control subject was obtained from the University Medical Center St Radboud, Nijmegen, the Netherlands. The samples were collected with full clearance from their Medical Ethics Committee. The frozen brain tissue was used for Western blot and quantitative real time PCR analysis and for making paraffin-embedded sections for histochemistry and immunohistochemistry tests.

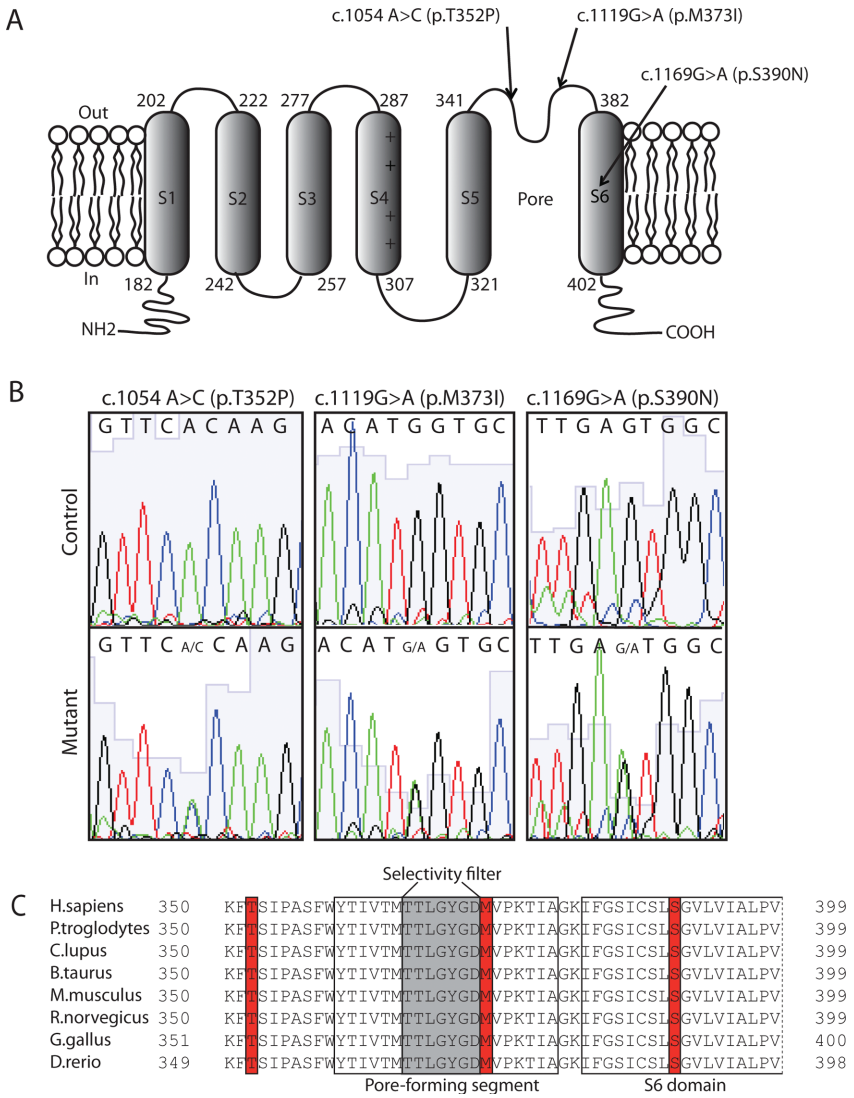

FIGURE 1: Spinocerebellar ataxia (SCA) 19 mutations lead to amino acid substitutions in highly conserved parts and domains of Kv4.3. (A) Schematic representation of the Kv4.3 channel and the location of the 3 SCA19 mutations. Segments (S) 1 to 4 form the voltage sensor domain, and S5 and S6, together with the pore loop, form the ion-selective pore. Positively charged residues in S4 detect the voltage change. The numbers indicate the amino acid numbers defining the beginning and end of the transmembrane segments. The c.1054 A>C (p.T352P) mutation is located in the third extracellular loop; the c.1119 G>A (p.M373I) and c.1169 G>A (p.S3900) mutations are located in the channel pore and the S6 transmembrane domain, respectively. (B) Electropherograms of the wild-type and mutant DNA sequences (NM_172198). (C) Amino acid comparison of Kv4.3 channels across species reveals that amino acids T352, M373, and S390 are 100% conserved from human to fish.

Plasmids

Wild-type *KCND3* cDNA cloned into the pCMV6 plasmid (short isoform; 636 amino acids, NM_172198) was purchased from Origene (Rockville, MD). The cDNA was amplified using primers (Supplementary Table 2) containing XhoI and EcoRI, or EcoR1 and EcoRV sites, to facilitate cloning into pcDNA3.1(−), and pIRES-EGFP/Cherry plasmids, respectively. The PCR product was first subcloned into pJET1.2/blunt (Fermentas, Vilnius, Lithuania). Mutations were introduced into the pJET-*KCND3* cDNA using side-directed mutagenesis (for primers see Supplementary Table 3) followed by further subcloning into pcDNA3.1(−) and pIRES-EGFP/Cherry. The pcDNA3.1-Kv4.3 plasmids were used for Western blot and immunohistochemistry and the pIRES-Kv4.3-EGFP/mCherry plasmids for patch-clamping. The constructs were checked for correctness by direct sequencing. The Emerald-C1 and Emerald-rat Kv channel interacting protein (KChIP) 2b/c plasmids were kindly provided by Dr K. Takimoto (Nagaoka University of Technology, Kamitomioka, Japan).[24]

Cell Culture and Transfection

HeLa and HEK293T cells were grown in Dulbecco's Modified Eagle's Medium (Invitrogen, Carlsbad, CA) supplemented with 10% fetal bovine serum (Invitrogen) and 1% Penicillin-Streptomycin (Gibco, Rockville, MD) in a 37°C incubator with 5% CO_2. Cells were grown in 6-well plates for Western blot, or on

glass cover slips in 24-well plates for immunocitochemistry and single-cell patch clamping for 24 hours following transfection with polyethylenimine (Polysciences, Warrington, PA), according to the manufacturer's instructions.

Western Blot

After 48 hours of transfection, cell extracts and human cerebella were homogenized using a 2% sodium dodecyl sulfate (SDS)/phosphate-buffered saline (PBS) buffer containing protease inhibitor cocktail (Roche Diagnostics, Indianapolis, IN) and sonicated. Cell and tissue lysates were centrifuged for 10 minutes at 13,000 rpm. Proteins were quantified using the BCA kit (Thermo Fisher Scientific, Rockford, IL), and the supernatant was mixed with loading sample buffer containing 10% β-mercaptoethanol and incubated for 5 minutes at 65°C.

For protein analysis, 50μg of cell extract or 200μg of brain proteins was loaded on 10% SDS-polyacrylamide gel electrophoresis gel followed by immunoblot analysis. Nitrocellulose membranes were incubated with mouse anti-Kv4.3 (K75/41; NeuroMab, Davis, CA; 1:1,000), mouse anti-calbindin (Abcam, Cambridge, UK; 1:2,500), mouse anti-actin (MP Biochemicals, Solon, OH; 1:5,000), mouse anti-p53 (Santa Cruz Biotechnology, Santa Cruz, CA; 1:1,000), and mouse anti-KChIP2 (Abcam; 1:1,000). Final quantification was performed using the program Quantity One (Bio-Rad).

Immunochemistry and Sevier–Munger Silver Staining

After 48 hours of transfection, HeLa cells were used for immunocytochemistry as previously described but with some modifications.[25,26] Briefly, cells were fixed with PBS containing 4% paraformaldehyde for 15 minutes, permeabilized, and blocked with 10% bovine serum albumin 0.1% Triton X-100 in PBS for 1 hour at room temperature. Primary and secondary antibodies were diluted in blocking buffer and incubated overnight at 4°C and 1 hour at room temperature, respectively. The antibodies used were: mouse anti-Kv4.3 (K75/41; NeuroMab; 1:250), rabbit anti-calnexin (Sigma, Milwaukee, WI; 1:200), FITC-conjugated goat anti-rabbit, and Cy3-conjugated anti-mouse (both 1:500; Jackson ImmunoResearch, West Grove, PA).

Cerebellar immunohistochemistry was performed on human cerebellar tissue 10μm thick sections embedded in paraffin. After deparaffination, rehydration, and antigen retrieval, tissues were blocked with 10% normal goat serum in Tris-buffered saline for 1 hour at room temperature. Primary and secondary antibodies were diluted in blocking buffer and incubated overnight at 4°C in a humidified chamber and for 2 hours at room temperature, respectively. The antibodies used were: rabbit anti-Kv4.3 (Alomone Labs, Jerusalem, Israel; 1:100) and mouse anti-calbindin (Abcam; 1:200), FITC-conjugated goat anti-mouse, and Cy3-conjugated goat anti-rabbit (1:500, Jackson ImmunoResearch). All the slides were mounted in Vectashield medium with 4′,6-diamidino-2-phenylindole (Vector Laboratories, Burlingame, CA).

For the silver staining, after deparaffination and rehydration, the cerebellar slides were placed in a 20% solution of AgNO3 for 20 minutes at 60°C. After rinsing in distilled water, the slides were placed in a solution of 10% AgNO3 (to which ammonia was added until the precipitate was dissolved) + 1 ml of 25% sodium carbonate solution. The solution was stirred while drops of 3.7% formalin were added until the slides stained golden brown. After being rinsed in distilled water, the slides were placed in 5% sodium thiosulfate solution for 2 minutes. Then the slides were rinsed again, followed by dehydration, xylene, and mounting.

Membrane Localization Scoring Assay

The percentage of transiently transfected HeLa cells with Kv4.3 membrane localization versus cells without membrane localization was scored using a Leica DM IRB inverted fluorescent microscope (Leica, Mannheim, Germany). The scoring assay was decoded and performed in triplicate by an independent scorer. On average, a minimum of 250 cells were counted per experiment.

Electrophysiological Measurements

Whole-cell patch clamp recording was used to quantify Kv4.3 potassium currents. All the experiments were performed at room temperature (22–24°C) using an Axopatch 200B amplifier, a Digidata 1320 A interface, and pClamp version 8.2 software (Axon Instruments, Foster City, CA). The extracellular (bath) solution contained (mmol/l) 140 NaCl, 4 KCl, 5 glucose, 2 $CaCl_2$, 1 $MgCl_2$, and 10 N-2-hydroxyethylpiperazine-N′-2-ethanesulfonic acid (HEPES), and the pH was adjusted to 7.4 with NaOH. The pipette solution contained (mmol/l) 140 KCl, 10 ethylenediaminetetraacetic acid, 1 $CaCl_2$, 1 $MgCl_2$, and 10 HEPES, and the pH was adjusted to 7.2 with KOH. Microelectrodes were made of GC120F-10 borosilicate glass (Harvard Apparatus, Holliston, MA) and pulled on a P-87 puller (Sutter Instruments, Novato, CA) having a final resistance of 4 to 5MΩ. Series resistance was compensated by 80 to 85%. Currents were filtered at 5 kHz and digitized at 10 kHz. Data were analyzed using Clampfit (Axon Instruments, Sunnyvale, CA) and Excel software (Microsoft, Redmond, WA).

Results

To identify the causative gene for SCA19, the genomic DNA of 2 affected individuals from our large Dutch family (IV:1 and III:10 in pedigree 1 and indicated with an *asterisk* in Supplementary Fig 1A) was analyzed by whole exome capturing. An average of 3GB of sequence was generated per individual, with an average coverage depth of 70× per targeted base. At least 85% of the total target region was covered >20×. The data were filtered for single nucleotide polymorphism (SNPs) that were not previously reported to dbSNPv132 or found in the 1000 Genomes Project (phases 1, 2, and 3), yielding 4,382 and 5,830 novel SNPs per individual (Supplementary Table 4).

Because the SCA19 disease gene had already been mapped to 1p21-q21, further analysis focused on those variations shared between the 2 SCA19 cases from the

large Dutch pedigree and present within the linkage interval. This analysis resulted in a total of 33 shared SNPs not reported in any database (Supplementary Table 5). Of these, 25 SNPs were detected in a heterozygous state (Supplementary Tables 6 and 7). After exclusion of the noncoding variants, validation by Sanger sequencing, a cosegregation check with the disease phenotype in the original SCA19 family (Supplementary Fig 1A), and screening of 400 Dutch blood bank controls, only one heterozygous missense T>G variation located at chromosome 1:112,524,295 remained unique for SCA19 (Supplementary Table 7). This variation led to a c.1054 A>C (p.T352P) substitution in the third extracellular loop of the voltage-gated potassium channel *KCND3*, also known as Kv4.3 (Fig 1A, B).

To obtain further genetic evidence for *KCND3* as the gene underlying SCA19, we screened 230 Dutch ataxia cases with no mutation in the known SCA genes (SCA1–3, 6, 7, 14, 17, and 23) by high-resolution melting. This ataxia cohort contains 30 cases with an autosomal dominant (AD) inheritance pattern and 200 cases with an unknown family history. In the probands of 2 AD families (pedigrees 2 and 3 in Supplementary Fig 1B, C), we identified 2 novel mutations, c.1119 G>A (p.M373I) and c.1169 G>A (p.S390N), located in the channel pore and the S6 transmembrane domain (Fig 1A, B), respectively. The c.1119 G>A mutation was detected in 2 affected individuals and in 1 apparently asymptomatic carrier (Supplementary Fig 1B). The segregation of the other mutation c.1169 G>A could not be tested due to unavailability of family members (Supplementary Fig 1C). All 3 mutated residues of human Kv4.3 are 100% conserved between different species (Fig 1C). None of the *KCND3* mutations was found in 800 Dutch control chromosomes, nor in several genetic databases (dbSNPv132, 1000 Genomes Project, and Exome Variant Server [National Heart, Lung, and Blood Institute Exome Sequencing Project, http://evs.gs.washington.edu/EVS/]).

The M373I proband (pedigree 2: II:1; Supplementary Fig 1B) had ambiguous neurological signs on testing at the age of 44 years. At age 52 years, he was re-examined but was found to be without neurological symptoms. His father (I:1) had a progressive gait disorder from age 55 years onward, including clear dysarthria, as well as ataxia of the arms and of gait. Computer tomography at that time demonstrated mild cerebellar atrophy. Comorbid conditions included hearing impairment and vascular atherosclerotic disease. He died at age 80 years. This paternal father was said to have had gait instability as well from about age 60 years onward, deceasing at age 90 years. Of the proband's sisters, the eldest was found to have very mild gait impairment at age 64 years, with equivocal dysdiadochokinesia of the hands (II:3). The youngest sister was unaffected (II:2).

The S390N proband (pedigree 3: II:1; Supplementary Fig 1C) suffered from a slowly progressive, spastic ataxic syndrome, including dysarthria, saccadic eye movements and downbeat nystagmus, cognitive impairment, and hearing deficits. The disease symptoms started between 30 and 35 years of age. A magnetic resonance imaging scan of the brain revealed cerebellar vermis atrophy. In addition, his brother and mother were diagnosed with the same disease.

Kv4.3 has been reported to be expressed in the cerebellum,[14,26] and immunohistochemistry of autopsy material from control cerebellum revealed a weak, punctuated staining of the Purkinje cell (PC) bodies, whereas a more intense Kv4.3 signal in larger puncta was observed in the soma of T352P mutant PCs (Fig 2A). Sevier–Munger silver staining revealed many empty baskets indicative of PC loss (Fig 2B). The anterior part of the vermis was most severely affected, followed by the posterior vermis and the cerebellar hemisphere. The PC loss in the hemisphere had a more patchy appearance. The cerebellar tonsils were the least affected. In this same order of PC loss, we observed degeneration/atrophy in both the molecular and internal granular layers. In the areas with remaining PCs, axonal torpedoes were observed. In addition, Kv4.3 protein levels in cerebellar lysates were lower in the patient's sample, which seemed to be the result of PC loss as shown by the reduced PC-specific marker calbindin expression (Fig 2C-E).

In episodic ataxia type 2, missense mutations have already been reported as causing ER retention of the α-subunit $Ca_v2.1$ of the P/Q voltage-activated calcium channel.[27] We therefore assessed whether the SCA19 missense mutations (T352P, M373I, and S390N) would also affect the subcellular localization/maturation of Kv4.3. Confocal microscopic analysis of transiently transfected HeLa cells revealed that, unlike wild-type Kv4.3 that was mainly located on the plasma membrane (74.5 ± 3.5%; Supplementary Fig 2), all 3 mutant proteins showed almost no or markedly reduced cell surface expression (T352P, 4.9 ± 0.6%; M373I, 40.4 ± 6.7%; S390N, 5.0 ± 2.7%; Supplementary Fig 2), but rather accumulated in perinuclear foci (Fig 3A). These data suggest that the SCA19 mutations cause ER retention of Kv4.3, causing impaired trafficking of the channel to the plasma membrane. Studies showed perfect colocalization of the SCA19 mutant Kv4.3 foci and the ER marker calnexin, but not with wild-type Kv4.3 (Fig 3B). In addition, all the Kv4.3 mutants were more rapidly degraded, upon inhibition of protein synthesis, than wild-type Kv4.3 (Fig 3C, D). The remaining Kv4.3 protein after 9 hours of cycloheximide treatment was 54 ± 10% for wild-type versus 15 ± 3%, 27 ±

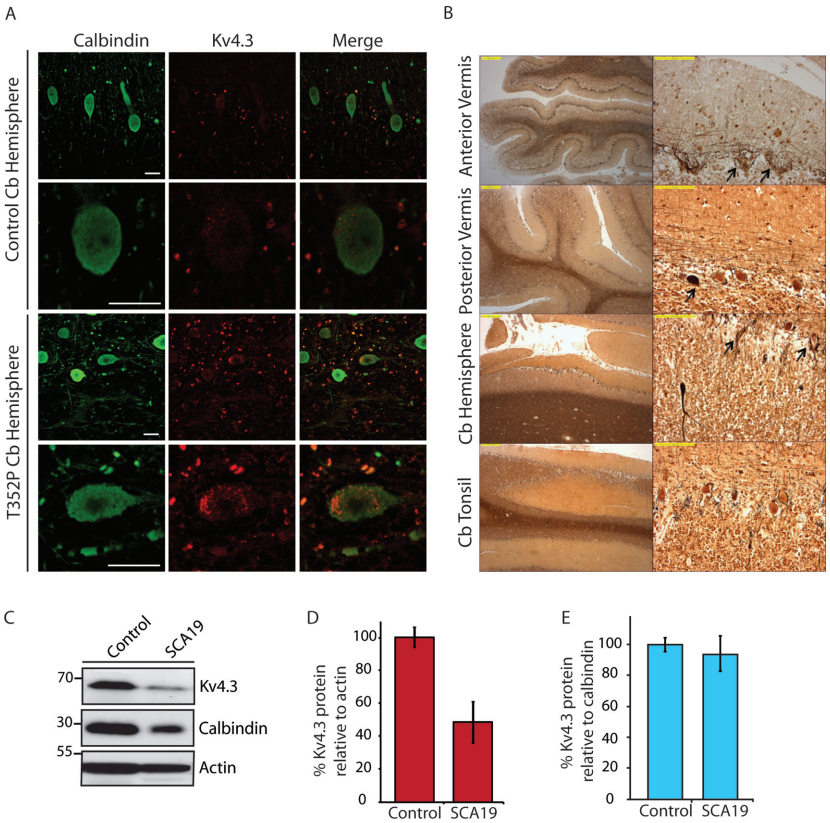

FIGURE 2: Immunohistochemistry, and Western blot analysis demonstrate the effect of the T352P mutation on Kv4.3 protein expression and cerebellar degeneration in human autopsy material. (A) Control cerebellar sections stained with antibodies against Kv4.3 (in red) and calbindin (in green) showed punctuated staining of the Purkinje cell (PC) bodies. Stronger and more accumulated Kv4.3 staining was observed in PC soma of the spinocerebellar ataxia (SCA) 19 cerebellum of a T352P patient. Scale bars = 25μm. (B) Micrographs of Sevier–Munger silver stainings showing overviews (left-hand side) and details (right-hand side) of degenerating cerebellar cortex. Note the atrophy of the folia in the vermis with empty baskets or torpedoes *(arrows)*. The cerebellar hemisphere was less affected, although empty baskets and torpedoes *(arrows)* were still encountered. The cerebellar tonsils were least affected and showed relatively normal numbers of PCs. Scale bars: left = 500μm, right = 100μm. (C) Western blot analysis of cerebellar protein extracts of control and T352P Kv4.3 mutant cerebella demonstrated markedly reduced Kv4.3 and calbindin protein levels. (D) Quantification of Kv4.3 protein levels in both control and T352P mutant cerebella. Data are normalized against actin levels using Quantity One. (E) Data normalized against calbindin levels.

10%, and 16 ± 4% for T352P, M373I, and S390N mutant Kv4.3, respectively. The cycloheximide treatment led to an efficient translational block, as was demonstrated using Western blot analysis against p53 (Supplementary Fig 3). This suggests that the SCA19 mutant proteins are recognized as misfolded proteins and are subsequently degraded, most likely via ER-associated degradation (ERAD).

Functional channels do not comprise Kv4.3 alone, because tetrameric Kv4.3 complexes form a hetero-octamer complex together with the regulatory β subunits, KChIPs, in which KChIPs drive the complex formation.[28,29] Because KChIPs are absent in HeLa cells, we wondered whether coexpression of Kv4.3 together with KChIP could improve the ER–Golgi-plasma membrane trafficking of the Kv4.3 mutants, as was seen for wild-type Kv4.3 (Fig 4). On expression of KChIP2b, but not of its inactive isoform KChIP2c, T352P and M373I (88.8 ± 1.5% and 82.6 ± 1.0%) were now detected at the plasma membrane like wild-type Kv4.3 (87.8 ± 0.4%; Supplementary Fig 2). However, the mislocalization of the S390N Kv4.3 mutant could not be rescued by coexpression of KChIP2b, as only 21.2 ± 8.4% of the cells showed cell surface expression, but rather trapped the regulatory β subunit in the same intracellular compartment (Fig 4A-D). In addition, KChIPs not only drive the tetramerization of Kv4.3 subunits, but they also regulate Kv4.3 protein expression and stability.[30,31] KChIP2b coexpression led to increased protein expression for all Kv4.3 proteins (Fig 4E) and also clearly improved the protein stability of wild-type, T352P, and M373I mutant Kv4.3 with the exception of S390N (Fig 4F,G). The remaining Kv4.3 protein levels after 9 hours of cycloheximide treatment were 96 ± 4% for wild-type

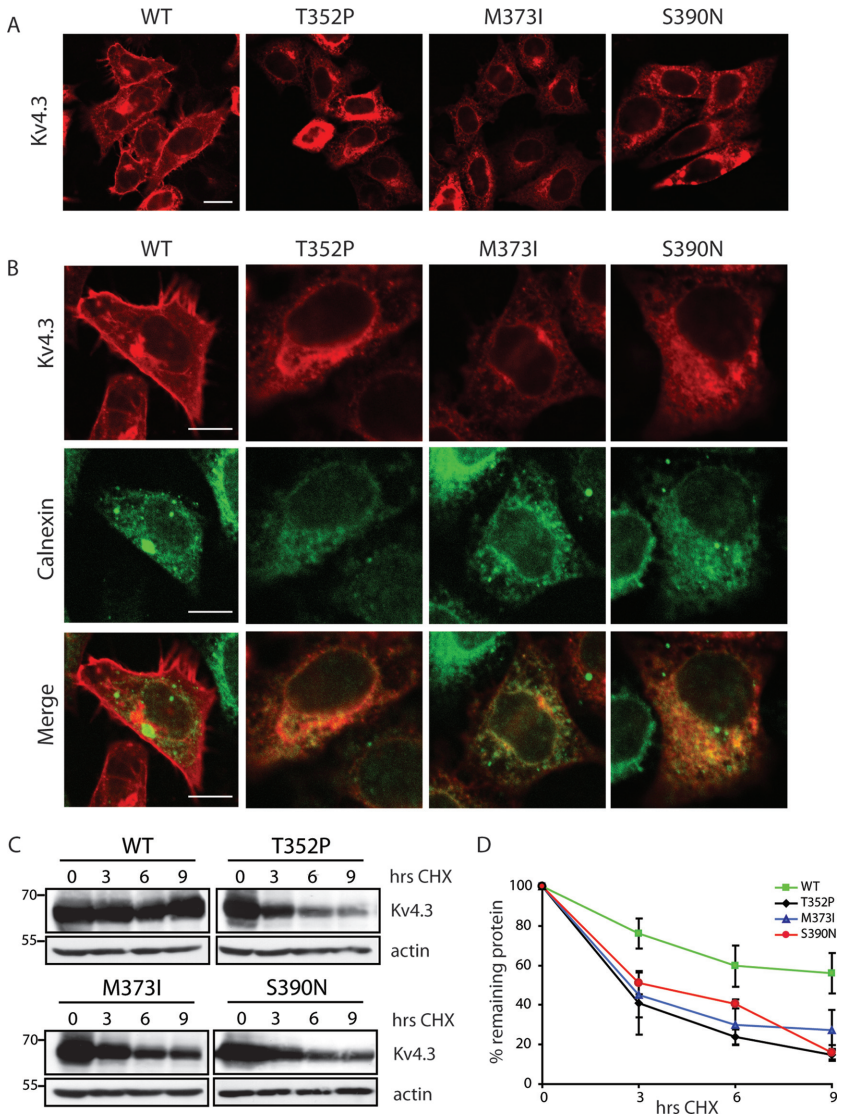

FIGURE 3: Endoplasmic reticulum (ER) retention and enhanced protein degradation of SCA19 mutant Kv4.3. (A) Confocal images of HeLa cells expressing wild-type (WT) or T352P, M373I, and S390N mutant Kv4.3 subunits. All Kv4.3 mutants clearly showed intracellular retention in the perinuclear region with only 4.9% (T352P), 40.4% (M373I), and 5.0% (S390N) membrane-expressing cells, whereas the WT Kv4.3 channel was mainly expressed on the cell surface (74.5% of the cells) detected using anti-Kv4.3 (in red). The quantification of the membrane localization is shown in Supplementary Fig 2. (B) Colocalization with the ER marker calnexin (in green) revealed that all T352P, M373I, and S390N mutant Kv4.3 proteins (in red) were retained in the ER, as was shown by the merged picture (in yellow). Scale bars = 20μm. (C) Time course protein degradation experiments were performed in HeLa cells transfected with either WT or T352P, M373I, and S390N mutant Kv4.3 treated with the protein synthesis inhibitor cycloheximide (CHX; 100μg/ml) for the indicated time periods, and the existing cellular pool of all Kv4.3 was detected by Western blot. The pool of T352P, M373I, and S390N mutant Kv4.3 proteins was degraded more rapidly than WT Kv4.3, which is a characteristic of misfolded ER-retained proteins. (D) Quantification of the Western blot degradation experiment normalized by actin, showing the percentage of remaining protein in time. The graphs show the average of 3 independent experiments, and the error bars represent the standard deviation (SD; mean ± SD).

Kv4.3 and 93 ± 20%, 87 ± 3%, and 13 ± 3% for T352P, M373I, and S390N, respectively. These data indicate that KChIP2b can ameliorate the folding defect of the SCA19 mutant proteins (except that of S390N) and thereby prevent protein degradation.

To test for Kv4.3 channel activity in the presence of KChIP2b, we recorded their K^+ currents by patch clamping in HEK293T cells. Activation of the wild-type Kv4.3–KChIP2b complex was detected at approximately −40 mV followed by more positive potentials up to +28 mV Fig 5A. In contrast, almost no detectable channel activity was detected for T352P–KChIP2b Fig 5B or (B) and S390N–KChIP2b Fig 5D or (D) complexes (1% and 13% channel activity compared to wild type [100%]), whereas strongly reduced activity (up to 75%) was measured for M373I–KChIP2b Fig 5C or (C). All

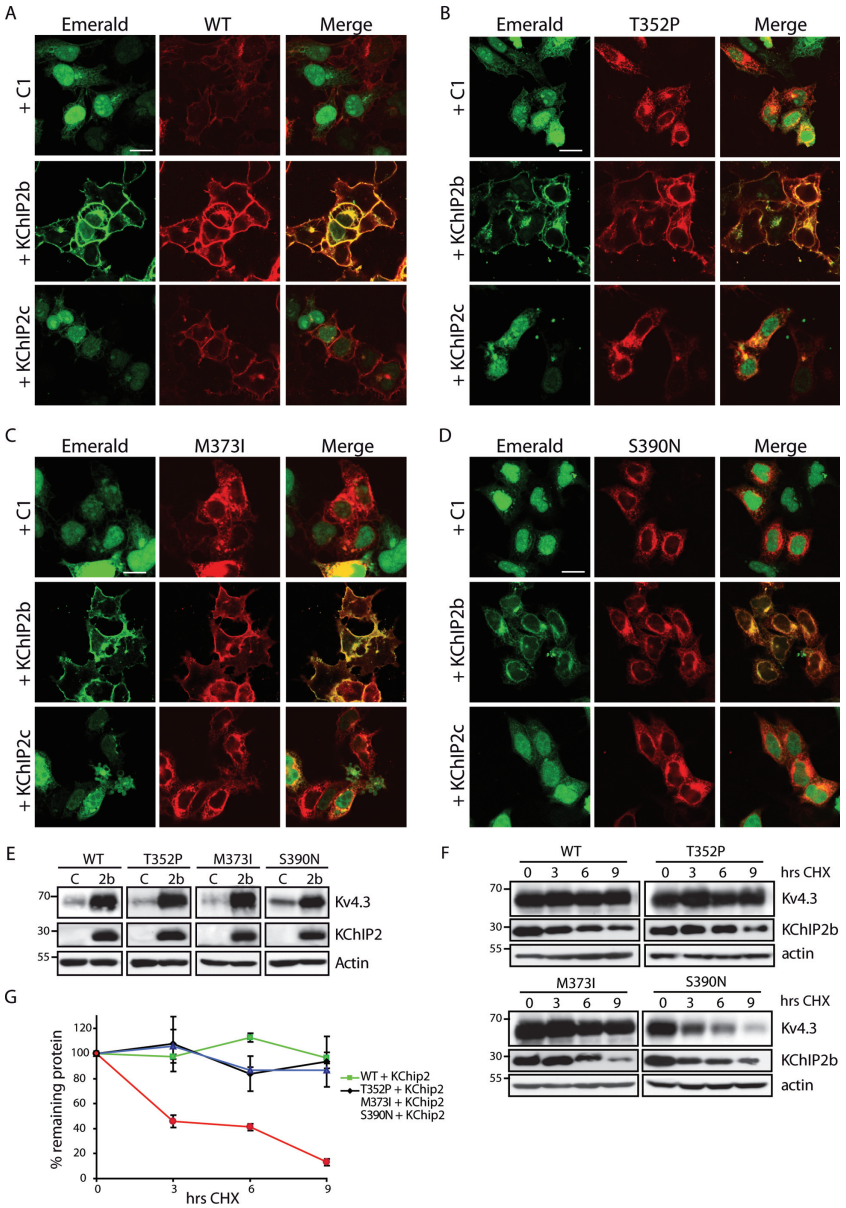

FIGURE 4: The regulatory β subunit Kv channel interacting protein 2b (KChIP2b) rescues the trafficking and stability of T352P and M373I mutant Kv4.3 channels. (A–D) Confocal images of HeLa cells expressing wild-type (WT) or T352P, M373I, and S390N mutant Kv4.3 subunits detected using anti-Kv4.3 antibody (in red), coexpressed with either empty control Emerald-C1 (Emd), Emd-KChIP2b, or the nonfunctional isoform Emd-KChIP2c (in green). Only KChIP2b expression resulted in a marked change in subcellular distribution of T352P (B) and M373I (C) mutant Kv4.3, as the remaining intracellular Kv4.3 pool was no longer associated with the endoplasmic reticulum, but showed a significant increase in cell surface expression up to 88.8% (T352P) and 82.6% (M373I) of cells (merge in yellow). (D) In contrast, almost no effect of KChIP2b on the subcellular distribution of S390N mutant Kv4.3 was detected, as now only 21.2% of cells showed Kv4.3 cell surface expression. The quantification of the membrane localization is shown in Supplementary Fig 2. Scale bars = 20μm. (E) Western blot data showed that KChIP2b is able to regulate the expression levels of WT and all spinocerebellar ataxia 19 mutant Kv4.3 proteins in HeLa cells, as for all Kv4.3 proteins increased Kv4.3 levels were detected in the presence of KChIP2b. C = empty control Emerald-C1; 2b = KChIP2b. (F) Time course for Kv4.3 protein degradation experiment. Western blot showed that coexpression of WT, T352P and M373I mutant Kv4.3 with KChIP2b resulted in a significant increase in protein stability (rescue up to almost 90% for WT, T352P and M373I mutant Kv4.3) in HeLa cells during 9 hours of cycloheximide (CHX) treatment. This effect was not observed for S390N mutant Kv4.3. Here, coexpression with KChIP2b led to about 13% rescue, and thus there was a similar percentage of remaining S390N mutant Kv4.3 proteins levels without KChIP2b after 9 hours of CHX treatment. (G) Quantification of the Kv4.3 protein degradation in the presence of KChIP2b normalized by actin using Quantity One. The graphs show the average of 3 independent experiments, and the error bars represent the standard deviation (SD; mean ± SD).

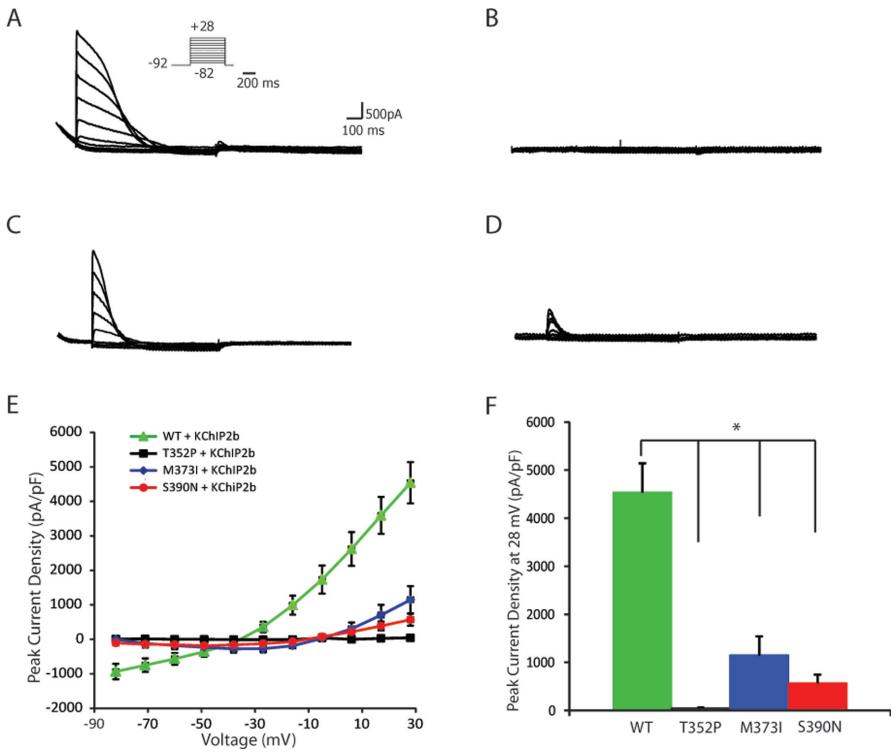

FIGURE 5: SCA19 mutations cause loss of Kv4.3-channel interacting protein (KChIP2b) channel complex activity and lead to reduced outward K^+ currents. (A–D) Representative whole cell potassium currents recorded in HEK293T cells transfected with wild-type WT (A), T352P (B), M373I (C), and S390N (D) mutant Kv4.3 coexpressing KChIP2b. The traces are generated by step depolarization of 200-millisecond duration from a holding potential of −82 mV to +28 mV. (E) The current–voltage relationship for WT, T352P, M373I, and S390N mutant Kv4.3–KChIP2b complexes. Clearly, the T352P, M373I, and S390N mutant Kv4.3–KChIP2b complexes showed almost no or strongly reduced channel activity. All values shown in the graph are the average of at least 10 independent measurements, and the error bars represent the standard error of the mean (SEM; mean ± SEM). (F) The bar graph shows the mean peak current density at 28 mV for WT, and T352P, M373I, and S390N mutant Kv4.3–KChIP2b complexes. All mutant–KChIP2b complexes showed significant reduced peak current density at 28 mV when compared to WT Kv4.3–KChIP2b. pA/pF, picoamperes per picofarad. The significance was calculated using Student's t-test (*p<0.05).

mutant Kv4.3 complexes showed significantly decreased current amplitude at 28 mV from 4,541 ± 599 (wild-type), to 44 ± 27 (T352P), 1,150 ± 393 (M373I), and 571 ± 174 (S390N) Fig 5E, F. These results demonstrate that although T352P mutant Kv4.3 and the regulatory β subunit KChIP2b coassemble and are present at the plasma membrane, the T352P–KChIP2b complex is not functional. The M373I–KChIP2b complex seems to be functional, but it produces Kv4.3 channels with marked reduced activity. Notably, very weak S390N–KChIP2b activity was detected, despite approximately all S390N–KChIP2b complexes being ER-retained, as was observed by microscopy. Therefore, we speculate that probably a few S390N–KCHIP2b complexes escape the ER and reach the plasma membrane but still yield almost no Kv4.3 channel activity. To confirm that the observed loss of channel activity is not due to enhanced T352P, M373I, or S390N Kv4.3 protein degradation, the Kv4.3 expression levels were checked using Western blot. No differences in expression levels were observed between wild-type and all mutant Kv4.3 subunits (Supplementary Fig 4).

Discussion

Our studies provide evidence that missense mutations in *KCND3* cause SCA19 by either altering Kv4.3 ER–Golgi plasma membrane transport, leading to enhanced protein degradation possibly by ERAD, and/or by loss of Kv4.3 channel functioning. *KCND3* encodes for Kv4.3, a highly conserved Shal-related subfamily, voltage-gated potassium channel, that is known to regulate cardiac and neuronal membrane excitability.[32] *KCND3* mRNA is highly expressed in cerebellum, including PCs, basket cells, stellate cells, and deep neurons,[33] and is thought to be important for its development.[14,34] The Kv4 channel family consists of 3 pore-forming α subunits, Kv4.1, Kv4.2, and Kv4.3.[35] These α subunits form tetrameric channel complexes and bind regulatory β subunits, KChIPs that change intracellular trafficking of the Kv4 channels from ER to plasma membrane and channel activity.[28,36] The neuronal Kv4 channel complex mediates the A-type K^+ current, which is important for dendritic excitability, somatodendritic signal integration, and long-term potentiation (LTP).[32,37–41]

KCND3 knockout mice have already been generated, but they do not display any neurological deficits,[42] probably due to redundancy of the other Kv4 family members. This implies that the SCA19 mutants described here must have a dominant negative action on the maturation and/or function of the other complex members and cause a loss of Kv4.3 function. Our S390N mutant data support such a hypothesis, as this mutant leads to the trapping of the regulatory β subunit in the ER.

The question remains how defects in a voltage-gated potassium channel can lead to cerebellar neurodegeneration. We are considering 3 potential mechanisms. First, altered dendritic excitability due to reduced A-type K^+ currents and subsequent initiation and a longer duration of action potentials might lead to changes of intracellular calcium homeostasis that may trigger PC death.[43] Second, SCA19 mutations could induce LTP deficits at the PC synapse. This would affect one of the important tasks of the cerebellum, fine adjustment of motor coordination, which requires intact long-term depression and LTP processes.[44,45] Third, the misfolded Kv4.3 channels may lead to a chronic form of ER stress and overinduction of the unfolded protein response, thereby activating proapoptotic factors leading to PC cell death.[46]

The different SCA19 mutations were found to affect Kv4.3 ER–Golgi plasma membrane maturation and channel activity differently, ranging from an almost complete inability to reach the plasma membrane (S390N) to almost complete absent (T352P) or only markedly reduced (M373I) channel activity. This may, to some extent, explain the diverse disease phenotypes observed in the 3 SCA19 families. The patients with the T352P and S390N mutations showed more severe disease phenotypes than those with the M373I mutation, given the presence of cognitive impairment, myoclonus, and tremor in most of the T352P patients, cognitive impairment and spasticity in the S390N case, and absence of these symptoms in M373I cases. In addition, the age of onset of the M373I family is relatively late (average of 55 years) compared to an average 30 or 35 years of age in the T352P and S390N cases.

Interestingly, the 3 different cellular phenotypes of the mutants are partially reminiscent of what is seen for mutations in the cyclic adenosine monophosphate–regulated chloride channel (CFTR) mutations that cause cystic fibrosis, and in which both CFTR maturation defects and reduced channel activities were also found.[47] Different therapeutic strategies that interfere with either the folding or degradation of maturation defective mutants or stimulate channel opening of membrane-associated mutants with impaired function may also be of value for the Kv4.3 mutants and are currently being investigated.

In addition to being expressed in brain, Kv4.3 is also expressed at relatively high levels in heart tissue. Although the SCA19 cases have not (yet) been reported to exhibit cardiomyopathy, it is notable that rare genetic variations have been associated with a gain of Kv4.3 function that is associated with Brugada syndrome,[48] implying that Kv4.3 may well play a role in human heart disease.

In conclusion, our current findings significantly contribute to revealing the importance of voltage-gated potassium channels in cerebellar ataxias, including EA type 1 and SCA13,[20,49] and show that mutations in *KCND3*, only required to prevent the fast repolarization of neurons, are sufficient to cause cerebellar neurodegeneration. We therefore speculate that more Kv4 family members or interacting proteins of Kv4.3 may also be involved in the etiology of other cerebellar ataxias.

Acknowledgment

This work was funded by a Rosalind Franklin Fellowship from the University of Groningen, the Prinses Beatrix Foundation (W.OR10-38), and NutsOhra (1101-042). Part of this work was performed at the University Medical Center Groningen Microscopy and Imaging Center, which is sponsored by the Netherlands Organization for Scientific Research (40-00506-98-9021 and 175-010-2009-023).

We thank all the patients for their participation, J. Senior for editing the manuscript, Dr K. Takimoto for providing the KChIP2 plasmids, and Dr B. van de Sluis for critically reading the manuscript.

Potential Conflicts of Interest

Nothing to report.

References

1. Durr A. Autosomal dominant cerebellar ataxias: polyglutamine expansions and beyond. Lancet Neurol 2010;9:885–994.
2. Bakalkin G, Watanabe H, Jezierska J, et al. Prodynorphin mutations cause the neurodegenerative disorder spinocerebellar ataxia type 23. Am J Hum Genet 2010;87:593–603.
3. Wang JL, Yang X, Xia K, et al. TGM6 identified as a novel causative gene of spinocerebellar ataxias using exome sequencing. Brain 2010;133:3510–3518.
4. Kobayashi H, Abe K, Matsuura T, et al. Expansion of intronic GGCCTG hexanucleotide repeat in NOP56 causes SCA36, a type of spinocerebellar ataxia accompanied by motor neuron involvement. Am J Hum Genet 2011;89:121–130.
5. Carlson KM, Andresen JM, Orr HT. Emerging pathogenic pathways in the spinocerebellar ataxias. Curr Opin Genet Dev 2009; 19:247–253.
6. Matilla-Duenas A, Sanchez I, Corral-Juan M, et al. Cellular and molecular pathways triggering neurodegeneration in the spinocerebellar ataxias. Cerebellum 2010;9:148–166.

7. Schorge S, van de Leemput J, Singleton A, et al. Human ataxias: a genetic dissection of inositol triphosphate receptor (ITPR1)-dependent signaling. Trends Neurosci 2010;33:211–219.
8. Verbeek DS, Schelhaas JH, Ippel EF, et al. Identification of a novel SCA locus (SCA19) in a Dutch autosomal dominant cerebellar ataxia family on chromosome region 1p21-q21. Hum Genet 2002; 111:388–393.
9. Chung MY, Lu YC, Cheng NC, Soong BW. A novel autosomal dominant spinocerebellar ataxia (SCA22) linked to chromosome 1p21-q23. Brain 2003;126:1293–1299.
10. Schelhaas HJ, Verbeek DS, van de Warrenburg BP, Sinke RJ. SCA19 and SCA22: evidence for one locus with a worldwide distribution. Brain 2004;127:E6.
11. Schelhaas HJ, Ippel PF, Hageman G, et al. Clinical and genetic analysis of a four-generation family with a distinct autosomal dominant cerebellar ataxia. J Neurol 2001;248:113–120.
12. Serodio P, Kentros C, Rudy B. Identification of molecular components of A-type channels activating at subthreshold potentials. J Neurophysiol 1994;72:1516–1529.
13. Tsaur ML, Chou CC, Shih YH, Wang HL. Cloning, expression and CNS distribution of Kv4.3, an A-type K+ channel alpha subunit. FEBS Lett 1997;400:215–220.
14. Serodio P, Rudy B. Differential expression of Kv4 K+ channel subunits mediating subthreshold transient K+ (A-type) currents in rat brain. J Neurophysiol 1998;79:1081–1091.
15. Li H, Durbin R. Fast and accurate long-read alignment with Burrows-Wheeler transform. Bioinformatics 2010;26:589–595.
16. McKenna A, Hanna M, Banks E, et al. The Genome Analysis Toolkit: a MapReduce framework for analyzing next-generation DNA sequencing data. Genome Res 2010;20:1297–1303.
17. DePristo MA, Banks E, Poplin R, et al. A framework for variation discovery and genotyping using next-generation DNA sequencing data. Nat Genet 2011;43:491–498.
18. Adamusiak T, Parkinson H, Muilu J, et al. Observ-OM and Observ-TAB: universal syntax solutions for the integration, search and exchange of phenotype and genotype information. Hum Mutat 2012;33:867–873.
19. Adzhubei IA, Schmidt S, Peshkin L, et al. A method and server for predicting damaging missense mutations. Nat Methods 2010;7: 248–249.
20. Waters MF, Minassian NA, Stevanin G, et al. Mutations in voltage-gated potassium channel KCNC3 cause degenerative and developmental central nervous system phenotypes. Nat Genet 2006;38:447–451.
21. Kumar P, Henikoff S, Ng PC. Predicting the effects of coding non-synonymous variants on protein function using the SIFT algorithm. Nat Protoc 2009;4:1073–1081.
22. Tavtigian SV, Deffenbaugh AM, Yin L, et al. Comprehensive statistical study of 452 BRCA1 missense substitutions with classification of eight recurrent substitutions as neutral. J Med Genet 2006;43:295–305.
23. Mathe E, Olivier M, Kato S, et al. Computational approaches for predicting the biological effect of p53 missense mutations: a comparison of three sequence analysis based methods. Nucleic Acids Res 2006;34:1317–1325.
24. Takimoto K, Yang EK, Conforti L. Palmitoylation of KChIP splicing variants is required for efficient cell surface expression of Kv4.3 channels. J Biol Chem 2002;277:26904–26911.
25. Duarri A, Lopez de HM, Capdevila-Nortes X, et al. Knockdown of MLC1 in primary astrocytes causes cell vacuolation: a MLC disease cell model. Neurobiol Dis 2011;43:228–238.
26. Strassle BW, Menegola M, Rhodes KJ, Trimmer JS. Light and electron microscopic analysis of KChIP and Kv4 localization in rat cerebellar granule cells. J Comp Neurol 2005;484:144–155.
27. Mezghrani A, Monteil A, Watschinger K, et al. A destructive interaction mechanism accounts for dominant-negative effects of misfolded mutants of voltage-gated calcium channels. J Neurosci 2008;28:4501–4511.
28. An WF, Bowlby MR, Betty M, et al. Modulation of A-type potassium channels by a family of calcium sensors. Nature 2000;403: 553–556.
29. Wang H, Yan Y, Liu Q, et al. Structural basis for modulation of Kv4 K+ channels by auxiliary KChIP subunits. Nat Neurosci 2007; 10:32–39.
30. Trimmer JS. Regulation of ion channel expression by cytoplasmic subunits. Curr Opin Neurobiol 1998;8:370–374.
31. Shibata R, Misonou H, Campomanes CR, et al. A fundamental role for KChIPs in determining the molecular properties and trafficking of Kv4.2 potassium channels. J Biol Chem 2003;278:36445–36454.
32. Hille B. Ionic channels in excitable membranes. 3rd ed. Sunderlands, MA: Sinauer Associates, 2001.
33. Hsu YH, Huang HY, Tsaur ML. Contrasting expression of Kv4.3, an A-type K+ channel, in migrating Purkinje cells and other post-migratory cerebellar neurons. Eur J Neurosci 2003;18:601–612.
34. Herrup K, Kuemerle B. The compartmentalization of the cerebellum. Annu Rev Neurosci 1997;20:61–90.
35. Covarrubias M, Bhattacharji A, De Santiago-Castillo JA, et al. The neuronal Kv4 channel complex. Neurochem Res 2008;33: 1558–1567.
36. Rhodes KJ, Carroll KI, Sung MA, et al. KChIPs and Kv4 alpha subunits as integral components of A-type potassium channels in mammalian brain. J Neurosci 2004;24:7903–7915.
37. Hoffman DA, Magee JC, Colbert CM, Johnston D. K+ channel regulation of signal propagation in dendrites of hippocampal pyramidal neurons. Nature 1997;387:869–875.
38. Birnbaum SG, Varga AW, Yuan LL, et al. Structure and function of Kv4-family transient potassium channels. Physiol Rev 2004;84: 803–833.
39. Kim J, Jung SC, Clemens AM, et al. Regulation of dendritic excitability by activity-dependent trafficking of the A-type K+ channel subunit Kv4.2 in hippocampal neurons. Neuron 2007;54:933–947.
40. Jerng HH, Pfaffinger PJ, Covarrubias M. Molecular physiology and modulation of somatodendritic A-type potassium channels. Mol Cell Neurosci 2004;27:343–369.
41. Chen X, Yuan LL, Zhao C, et al. Deletion of Kv4.2 gene eliminates dendritic A-type K+ current and enhances induction of long-term potentiation in hippocampal CA1 pyramidal neurons. J Neurosci 2006;26:12143–12151.
42. Niwa N, Wang W, Sha Q, et al. Kv4.3 is not required for the generation of functional Ito, f channels in adult mouse ventricles. J Mol Cell Cardiol 2008;44:95–104.
43. Spitzer NC. Electrical activity in early neuronal development. Nature 2006;444:707–712.
44. De Zeeuw CI, Yeo CH. Time and tide in cerebellar memory formation. Curr Opin Neurobiol 2005;15:667–674.
45. Jorntell H, Hansel C. Synaptic memories upside down: bidirectional plasticity at cerebellar parallel fiber-Purkinje cell synapses. Neuron 2006;52:227–238.
46. Doyle KM, Kennedy D, Gorman AM, et al. Unfolded proteins and endoplasmic reticulum stress in neurodegenerative disorders. J Cell Mol Med 2011;15:2025–2039.
47. Roomans GM. Pharmacological treatment of the ion transport defect in cystic fibrosis. Expert Opin Investig Drugs 2001;10:1–19.
48. Giudicessi JR, Ye D, Tester DJ, et al. Transient outward current (I(to)) gain-of-function mutations in the KCND3-encoded Kv4.3 potassium channel and Brugada syndrome. Heart Rhythm 2011;8:1024–1032.
49. Browne DL, Gancher ST, Nutt JG, et al. Episodic ataxia/myokymia syndrome is associated with point mutations in the human potassium channel gene, KCNA1. Nat Genet 1994;8:136–140.